Interstrand Loops CD and EF Act as pH-Dependent Gates To Regulate Fatty Acid Ligand Binding in Tear Lipocalin†

Oktay K. Gasymov, Adil R. Abduragimov, Taleh N. Yusifov, and Ben J. Glasgow*

Departments of Pathology and Ophthalmology, University of California at Los Angeles School of Medicine, Los Angeles, California 90095

Received May 6, 2004; Revised Manuscript Received July 23, 2004

ABSTRACT: Tear lipocalin (TL), a major component of human tears, shows pH-dependent endogenous ligand binding. The structural and conformational changes associated with ligand release in the pH range of 7.5−3.0 are monitored by circular dichroism spectroscopy and site-directed tryptophan fluorescence. In the transition from pH 7.5 to pH 5.5, the ligand affinity for 16-(9-anthroyloxy)palmitic acid (16AP) and 8-anilino-1-naphthalenesulfonic acid is reduced. At pH 4.0 these ligands no longer bind within the TL calyx. From pH 7.3 to pH 3.0, the residues on loops CD and EF, which overhang the calyx entrance, show reduced accessibility to acrylamide. In addition resonance energy transfer is enhanced between residues on the two loops; the distance between the loops narrows. These findings suggest that apposition of the loops at low pH excludes the ligand from the intracavitary binding site. The conformational changes observed in transition from pH 7.3 to pH 3.0 for loops CD and EF are quite different. The CD loop shows less population reshuffling than the EF loop with an acidic environment, probably because backbone motion is restrained by the adjacent disulfide bond. The Trp fluorescence wavelength maximum (λ_{max}) reflects internal electrostatic interactions for positions on loops CD and EF. The titration curves of λ_{max} for mutants on the EF loop fit the Hendersen−Hasselbalch equation for two apparent pK_a values, while the CD loop positions fit satisfactorily with one pK_a value. Midpoints of transition for the binding affinity of TL tryptophan mutants to 16AP occur at pH 5.5−6.1. Replacement of each amino acid on either loop by single tryptophan mutation does not disrupt the pH-dependent binding affinity to 16AP. Taken together the data suggest that pH-driven ligand release involves ionization changes in several titratable residues associated with CD and EF loop apposition and occlusion of the calyx.

Tear lipocalin (TL)[1] is a major component and the principal lipid-binding protein in tears. TL is promiscuous; endogenous ligands include an assortment of fatty acids, alkyl alcohols, glycolipids, phospholipids, and cholesterol (*1*). Putative functions for TL include scavenging lipid from the corneal surface to prevent the formation of lipid-induced dry spots (*2*), solubilization of lipid in tears (*2*), antimicrobial activity (*3*), cysteine proteinase inhibition (*4*), transport of sapid molecules in saliva (*5*), transport of retinol in tears (*6*), scavenging potentially harmful lipid oxidation products (*7*), transport of antioxidants in tears (*8*), and endonuclease activity (*9*). Common to most of these diverse functions is the binding of small hydrophobic ligands.

TL belongs to the lipocalin family of proteins that is characterized by a cup-shaped ligand-binding fold within a continuously hydrogen bonded β-barrel that is formed by eight antiparallel β-strands (*10*). The endogenous ligands of TL are known to bind in the lipocalin fold. Fatty acids, the best studied ligands of TL, are known to bind with the polar headgroup oriented toward solvent at the calyx mouth and the hydrocarbon tail buried in the cavity (*11*). Several features of TL may influence ligand binding and stability: the conserved disulfide bond (*12*), a hydrophobic cluster of conserved residues including proximate Trp17 and Phe99, and an external hydrophobic patch that includes Ile98 (*13*). The disulfide bond and hydrophobic regions confer restrictive influences on ligand binding for TL (*12*).

The size of the ligand also appears to be a limiting factor for binding to TL. The TL calyx is capacious compared to that of other lipocalins. DAUDA and 16-doxylstearic acid will bind in the cavity of TL but not in the cavity of β-lactoglobulin (*14*, *15*). However, the cavity of TL does not accommodate P646, which contains a large perylene group (*16*). A homology model of TL constructed from site-directed tryptophan fluorescent data may partially explain the promiscuous ligand binding (*17*). Residues with smaller side chains (Ala) are positioned in the calyx of TL at sites that correspond to larger side chain residues (Ile) in β-lactoglobulin. In addition, TL has short interstrand loops CD and EF that overhang the cavity entrance compared to other more selective lipocalins, such as retinol-binding protein.

The affinity of TL for an assortment of ligands is also influenced by changes in pH. The affinity of TL for both rifampin and spin-labeled lauryl amide is markedly reduced

† Supported by U.S. Public Health Service Grant EY-11224 and an unrestricted grant from Research to Prevent Blindness to B.J.G.

* To whom correspondence should be addressed. Fax: (310) 794-2144. Phone: (310) 825-6998. E-mail: bglasgow@mednet.ucla.edu.

[1] Abbreviations: ANSA, 8-anilino-1-naphthalenesulfonic acid; 16AP, 16-(9-anthroyloxy)palmitic acid; MTS-dansyl, dansylamidoethyl methanethiosulfonate; CD, circular dichroism; λ_{max}, fluorescent emission maximum; RBP, retinol-binding protein; TL, tear lipocalin; UV, ultraviolet; RET, resonance energy transfer.

10.1021/bi049076o CCC: $27.50
Published on Web 09/18/2004

at pH 3.0 versus pH 7.3 (*18*, *19*). At pH 3.0 fluorescent quenching of the single tryptophan in TL by endogenous lipids is markedly reduced and accompanied by a red shift compared to spectra at pH 7.3 (*19*). PH-dependent ligand binding may be functionally important for TL because the tear film is replete with negatively charged phospholipids that potentially create a steep pH gradient at lipid−water interfaces (*20*).

For some lipocalins, pH-dependent ligand binding may be related to movement of the interstrand loops that overhang the calyx mouth. In bovine β-lactoglobulin, acidic pH may trigger closure of the EF loop by protonation of Glu89. The calculated pK_a value for Glu89 of 5.59 correlates with the midpoint of transition for palmitic acid binding obtained by NMR (*21*, *22*). The effects are presumably mediated through a hydrogen-bonding network including Glu89 and local changes in structure that closes the loop and limits access to the calyx (*23*). Fatty acid binding to β-lactoglobulin increases from pH 6.2 to pH 8.3 (*24*). For another lipocalin, retinol-binding protein, pH-dependent retinol release is accompanied by significant alterations in a complex of salt bridges and hydrogen bonds with substantially lowered conformational stability. Serial changes in the charges of titratable groups are implicated in pH-induced conformational changes, which lead to increased ligand mobility and facilitated release of retinol (*25*).

The overall structure of TL is very close to that of β-lactoglobulin although the glutamic acid residue at the position corresponding to 89 is not present (*17*). Other titratable residues are candidates for pH-driven electrostatic interactions that may influence ligand binding. Specifically, titratable groups at pH 3.0−7.5 have been assigned to loops EF (Asp80) and CD (Glu63) in TL (*17*).

Several methods can be used to study protein structural and conformational changes with pH. The pK_a values of the titrating sites in a protein can be experimentally determined by NMR spectroscopy. Standard NMR methods are currently limited to proteins with molecular masses of ~30 kDa or less (*26*). Evidence suggests that TL forms a dimer (~35 kDa) at physiologic pH (*2*, *6*, *27*). An alternative to NMR spectroscopy is computer-based modeling to determine pK_a values of the ionizable groups in a protein (*21*), but the crystal structure is needed and as yet is unavailable for TL. A crystallographic approach to study pH-induced conformational changes may have limitations. For example, RBP is known to release its endogenous ligand, retinol, at pH 4.5 in solution (*28*). However, in crystallized holo-RBP the ligand remains bound and unaltered with the overall protein structure preserved even at a pH of 2.0 (*25*). This contradiction has been attributed to crystal packing forces that presumably impede unfolding and release. The conformational changes that a protein exhibits throughout an entire pH range are perhaps best studied in solution.

Tryptophan fluorescence is a powerful tool for probing proteins in solution. Parameters such as the fluorescence wavelength maximum (λ_{max}), fluorescence lifetimes, and energy transfer can be applied to folding/unfolding, substrate/ligand binding, accessibility to external quenchers, resolving secondary structure, and distance measurements between two residues. Site-directed mutagenesis, using tryptophan to replace a single amino acid in TL, may be done with minimal perturbation in structure and function (*17*, *29*). Recent advances in the fundamentals of tryptophan fluorescence provide the framework to understand the effects of local side chain interactions on tryptophan fluorescence including the assignment of fluorescence lifetimes to rotamer populations (*30*, *31*). Tryptophan fluorescence λ_{max} is very sensitive to nearby charges of side chains in proteins. Electron density is shifted from the pyrrole ring to the benzene ring upon excitation to the ^1L_a state, the fluorescent state in most proteins. Furthermore, titratable side chains in proximity to Trp should make an enormous change in λ_{max} during acid−base transitions that generate or annihilate charge. Titratable side chains at pH < 7 include Glu, Asp, and His. For Glu and Asp, protonation results in the loss of a negative charge. Protonation of His creates a positive charge. Therefore, a large shift of Trp fluorescence λ_{max} is expected with the protonation of nearby Glu, Asp, and His. Complementary information is available from fluorescence lifetimes. Only protonated carboxylic acid side chains quench indole fluorescence. Neutral His is a relatively weak quencher, but positively charged His is one of the best quenchers. These interactions of tryptophan provide the basis to study the pH-dependent changes in structure, conformation, and ligand binding of TL in solution by spectroscopic methods.

The combination of fluorescent ligands ANSA and 16AP permits the indentification of binding modes and the functional characterization of ligand binding during pH titration. Attention is focused on the relative positions of the interstrand loops that overhang the calyx mouth. Site-directed mutagenesis is used to create reporter tryptophans and cysteines labeled with dansyl groups along both loops to monitor conformational changes, ligand binding, and interloop distances at varying pH. The studies show that movement of the loops CD and EF is associated with protonation of side chains in local environments and correlated with pH-dependent changes in ligand binding for TL.

EXPERIMENTAL PROCEDURES

Site-Directed Mutagenesis and Plasmid Construction. The TL cDNA in PCR II (Invitrogen, San Diego, CA), previously synthesized (*32*), was used as a template to clone the TL gene spanning bases 115−592 of the previously published sequence (*6*) into pET 20b (Novagen). Flanking restriction sites for *Nde*I and *Bam*HI were added to produce the native protein sequence as found in tears (*33*). To construct mutant proteins with a single tryptophan, the previously well characterized TL mutant, W17Y, was prepared with oligonucleotides (Universal DNA Inc.) by sequential PCR steps (*34*, *35*). Using this mutant as a template, mutant cDNAs were constructed in which the corresponding amino acids were additionally substituted sequentially with tryptophan. Amino acid 1 corresponds to His, bases 115−118 according to Redl (*6*). Single Trp mutants include W17Y/S58W (for simplicity denoted as W58), W17Y/G59W (W59), W17Y/R60W (W60), W17Y/Q62W (W62), W17Y/E63W (W63), W17Y/D80W (W80), W17Y/G81W (W81), W17Y/G82W (W82), and W17Y/K83W (W83). Mutants that have both a single Trp and a single Cys substitution include W17Y/C101L/Q62W/G81C (W62C81), W17Y/C101L/Q62W/G82C (W62C82), W17Y/C101L/E63W/D80C (W63C80), W17Y/C101L/V67W/G81C (W67C81), and W17Y/C101L/V67W/G82C (W67C82).

Expression and Purification of Mutant Proteins. The mutant plasmids were transformed in *Escherichia coli* BL 21 (DE3), the cells were cultured, and proteins were expressed purified and analyzed as previously described in the Supporting Information (*1*, *36*, *37*).

Absorption Spectroscopy. UV absorption spectra were measured at room temperature using a Shimadzu UV-2400PC spectrophotometer. The spectra were corrected for light scattering by plotting the dependence of the log of the absorbance of the solution versus the log of the wavelength and extrapolating the linear dependence between these quantities in the range 320−360 nm to the absorption range 240−320 nm.

CD Spectral Measurements. Spectra were recorded (Jasco 810 spectropolarimeter, 0.2 and 10 mm path length for far- and near-UV spectra, respectively) using protein concentrations of 1.2 mg/mL in 10 mM sodium phosphate (pH 7.5−5.5) or 30 mM sodium citrate (pH 4.0−2.0). Eight and sixteen scans from 190 to 260 nm and from 250 to 320 nm were averaged, respectively. Results were recorded in millidegrees and converted to mean residue ellipticity in deg cm^2 $dmol^{-1}$.

Urea-Induced Unfolding. Proteins, 1.2 mg/mL, were incubated with varying concentrations of urea at room temperature for 18 h. Circular dichroism spectra were obtained at room temperature. The fraction of unfolded protein was plotted as the fractional changes in ellipticity at 218 nm, $(\theta - \theta_n)/(\theta_u - \theta_n)$, versus progressively increasing concentrations of urea, where θ is the ellipticity observed and n and u refer to the native and unfolded states, respectively.

Fluorescence Labeling of TL Mutants. TL mutants containing cysteine were labeled with a 5× molar excess of the fluorescent label MTS-dansyl (TRC Inc., North York, Ontario, Canada) in buffer 10 mM NaP, pH 6.8, at 4 °C overnight. Free label was separated from the labeled protein by gel filtration on a desalting column (Pharmacia Biotech HiTrap, 5 mL). Absorption spectra were used to calculate the labeling efficiency for each mutant. Concentrations were calculated using extinction coefficient $\epsilon_{335} = 4100\ M^{-1}\ cm^{-1}$ for MTS-dansyl. The protein concentration was determined by the buret method. The efficiencies of labeling for all considered TL mutants were in the range of 0.98−1.02.

Fluorescence Binding Assays. Samples of 2 mL of each apoprotein, 1.6−2.1 μM in 10 mM sodium phosphate (pH 7.5−5.5) or 30 mM sodium citrate (pH 4.0−3.0), were titrated by addition of 16AP (Molecular Probes, Eugene, OR), and the fluorescence was measured at 450 nm, $\lambda_{ex} = 361$ nm. The concentration of an ethanol stock solution of 16AP was confirmed by absorbance at 361 nm, using extinction coefficient $\epsilon_{361} = 8200\ M^{-1}\ cm^{-1}$ (*35*). Following each addition of ligand, the solution was mixed and allowed to equilibrate for 4 min. Background fluorescence was corrected as described previously (*38*). Fluorescent intensities were corrected for dilution and inner filter effects. At the end of each titration experiment, the ethanol concentration did not exceed 2%. 16AP binding curves at low pH were noticeably sigmoidal, which denotes cooperative binding. Therefore, 16AP binding curves were fit to the Hill equation

$$y = \frac{F_{max} L^n}{K_d + L^n}$$

where F_{max} is the fluorescence maximum upon ligand saturation, L is the free ligand concentration, K_d is the apparent dissociation constant that corresponds to the ligand concentration at the half point transition of the fluorescence titration curve, and n is the degree of cooperativity.

Apo-TL (1.2 μM) was used for similar experiments performed with ANSA (Sigma), $\epsilon_{350} = 6300\ M^{-1}\ cm^{-1}$. The ANSA binding data were analyzed with the following formula for one binding site:

$$y = 0.5F\left[\left(1 + \frac{K_d}{nP} + \frac{L_t}{P}\right) - \left[\left(1 + \frac{K_d}{nP} + \frac{L_t}{nP}\right)^2 - \frac{4L_t}{nP}\right]^{1/2}\right] + cP$$

where F is a fluorescence scaling factor, K_d is the apparent dissociation constant, P is the total protein concentration, L_t is the total ligand concentration, c is the parameter that accounts for the contribution of nonspecific binding, and n is the stoichiometry.

Steady-State Fluorescence Spectroscopy. Steady-state fluorescence measurements were made on a Jobin Yvon-SPEX (Edison, NJ) Fluorolog tau-3 spectrofluorometer; the bandwidths for excitation and emission were 2 nm. The excitation λ of 295 nm was used to ensure that light was absorbed almost entirely by tryptophanyl groups. Protein solutions with about 0.05 OD at 295 nm were analyzed. All spectra were obtained from samples in 10 mM sodium phosphate (pH 7.5−5.5) or 30 mM sodium citrate (pH 4.0−2.0). Temperature was maintained at 24 °C with a thermojacketed cell holder. The fluorescence spectra were corrected for light scattering from the buffer and the instrument response using the appropriate correction curve. The details of quantum yield calculation are described in the Supporting Information.

Accessibility of the Trp Side Chain by Acrylamide Quenching of Fluorescence. The fluorescence of a protein, monitored at the emission maximum λ_{max}, was quenched by the progressive addition of small aliquots of an 8 M acrylamide solution as previously described (*29*). Correction for dilution of the sample and for inner filter effects caused by acrylamide absorption was performed as previously described (*39*). The quenching data were fit to the modified form of the Stern−Volmer relationship (*39*): $\{F_0\}/\{F = (1 + K_{sv}[Q])\}e^{V[Q]}$, where F_0 and F are the fluorescence intensities in the absence and presence of the quencher, respectively, [Q] is the concentration of quencher, V is the static quenching constant, and K_{sv} is the dynamic quenching constant ($K_{sv} = k_q\tau_0$). k_q is the bimolecular collisional rate constant and τ_0 the fluorescence lifetime in the absence of the quencher.

Fluorescence Lifetime Measurements. Time-resolved intensity decay data were obtained using a Jobin Yvon-SPEX Fluorolog tau-3 phase/modulation frequency domain fluorometer equipped with a continuous-wave laser (*13*). The instrument arrangement is detailed in the Supporting Information. The intensity decay data were analyzed in terms of the following multiexponential decay law:

$$I(t) = \sum \alpha_i \exp(-t/\tau_i)$$

where α_i and τ_i are the normalized preexponential factor and decay time, respectively. The fractional fluorescence intensity of each component is defined as $f_i = \alpha_i\tau_i/\sum\alpha_j\tau_j$.

The mean lifetime (intensity-averaged) was calculated as $\bar{\tau} = \sum f_i\tau_i$. For the calculation of the efficiency of RET the amplitude-averaged lifetime $\langle\tau\rangle = \sum\alpha_j\tau_j$ was used. The radiative rate constant was calculated as $k_r = \phi/\langle\tau\rangle$.

All single Trp mutant proteins showed lower fluorescence lifetimes at pH 3.0 compared to pH 7.3. To separate dynamic quenching of Trp fluorescence from that of reshuffling between the rotamer populations of Trp, ratios of two lifetimes were arranged as the following formula (*40*):

$$\frac{\langle\tau\rangle}{\langle\tau_0\rangle} = \frac{\sum\alpha_i\tau_{0i}}{\sum\alpha_{0i}\tau_{0i}}\frac{\sum\alpha_i\tau_i}{\sum\alpha_i\tau_{0i}} = f_{PR}f_{DQ}$$

where the subscript 0 refers to the reference state (lifetime parameter at pH 7.3) and f_{PR} and f_{DQ} represent population reshuffling and pure dynamic quenching, respectively. Because the determination of the fluorescence quantum yield is less accurate than that of the fluorescence lifetime, we did not use changes in the average radiative rate constant for analysis of Trp fluorescence.

Distance Measurements by RET. Resonance energy transfer between the Trp residue (donor) and the labeled dansyl group (acceptor) was used to determine the average distance in different conditions. The details of the calculation are shown in the Supporting Information.

Calculation of pK_a Values from Fluorescence λ_{max} Data. We made the assumption that pH-dependent changes in fluorescence λ_{max} are driven by the ionization state of titratable amino acid side chains in close proximity of the tested Trp. Therefore, pH titration data were analyzed by fitting the function derived from the Hendersen−Hasselbalch equation

$$\mathrm{pH} = \mathrm{p}K_a + \log\frac{[\text{conjugate base}]}{[\text{conjugate acid}]} = \mathrm{p}K_a + \log\frac{\theta}{1-\theta}$$

where θ represents the fractional concentration of the conjugate base. In rapid equilibrium conditions between protonated and unprotonated forms

$$\theta = \frac{\lambda_{max} - \lambda_{max}^{acid}}{\lambda_{max}^{base} - \lambda_{max}^{acid}}$$

$\lambda_{max}{}^{acid}$ and $\lambda_{max}{}^{base}$ represent fluorescence λ_{max} at the extremes of pH and were estimated from the fitting curve generated by substituting θ into the Hendersen−Hasselbalch equation:

$$\lambda_{max} = \frac{\lambda_{max}^{acid} + \lambda_{max}^{base} \times 10^{(\mathrm{pH}-\mathrm{p}K_a)}}{1 + 10^{(\mathrm{pH}-\mathrm{p}K_a)}}$$

For situations where two titrating groups are involved, the equation for the noninteracting model was used:

$$\lambda_{max} = \frac{\lambda_{max}^{acid} + \lambda_{max}^{int1} \times 10^{(\mathrm{pH}-\mathrm{p}K_a{}^1)} + \lambda_{max}^{base} \times 10^{(2\mathrm{pH}-\mathrm{p}K_a{}^1-\mathrm{p}K_a{}^2)}}{1 + 10^{(\mathrm{pH}-\mathrm{p}K_a{}^1)} + 10^{(2\mathrm{pH}-\mathrm{p}K_a{}^1-\mathrm{p}K_a{}^2)}}$$

where $\lambda_{max}{}^{int1}$ is an intermediate value. The data were fit with the nonlinear least-squares method using Origin 7.0 (Microcal, Northhampton, MD).

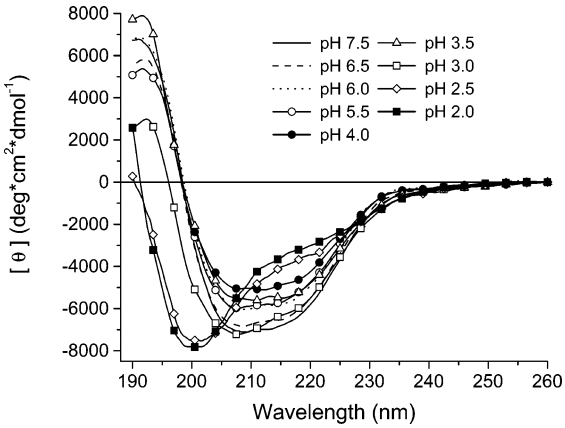

FIGURE 1: Far-UV CD spectra of apo-TL at various pH values.

RESULTS AND DISCUSSION

Circular Dichroism. Previous studies have shown that fatty acids bind TL at pH 7.3, and are released at pH 3.0. At pH 3.0, TL assumes a molten globule state (*19*). However, only two pH values, 3.0 and 7.3, were studied. To better determine structural changes within this pH range, the CD spectra were studied in pH titration experiments. The far-UV CD spectra of apo-TL at varying pH are shown in Figure 1. For the pH range 7.5−5.5, the minima of the CD spectra are about 208 and 214 nm with the maximum at about 192 nm. The minimum at 214 nm is characteristic of β-sheet structure. The minimum at 208 nm has been shown previously to occur in delipidated TL and is part of the fractional loss in β-structure and concomitant increase in random coil in the protein (*35*).

Within the pH range of 7.5−3.5, the similar shapes of the spectra indicate no significant alteration in secondary structure. At pH 3.0 there is a marked decrease in signal intensity at 192 nm although the general shape of the spectra is maintained. This change can be attributed to relaxation but not loss of secondary structure. However, at pH 2.0 and 2.5 there is a clear loss of β-sheet structure and an increased contribution from unordered structure. At pH 2.0 there is residual optical activity in the region >210 nm indicative of secondary structural elements; the acidic unfolding of the protein is not complete. Far-UV CD spectra were obtained for all of the Trp and Trp/Cys mutants over the entire pH range and found to be similar (see the Supporting Information).

The near-UV CD spectra provide a view of overall aromatic side chain conformational changes that occur with variation in pH for apo-TL (Figure 2). In the pH range 7.5−6.0 the spectra are almost identical. At pH 5.5 there is increased aromatic side chain asymmetry evident from the increased negative signal intensity from 270 to 295 nm. There is a gradual decrease in intensity of the CD signal from pH 5.5 to pH 3.5; the loss of signal intensity is enhanced at pH 3.0 and 2.5. By pH 2.0 a complete transition to a featureless spectrum is evident. The comparison of near- and far-UV CD spectra at various pH values indicates that a decrease in pH from 7.5 to 3.0 is accompanied by successive conformational changes attributed to decreased aromatic side chain rigidity but secondary structure elements are essentially

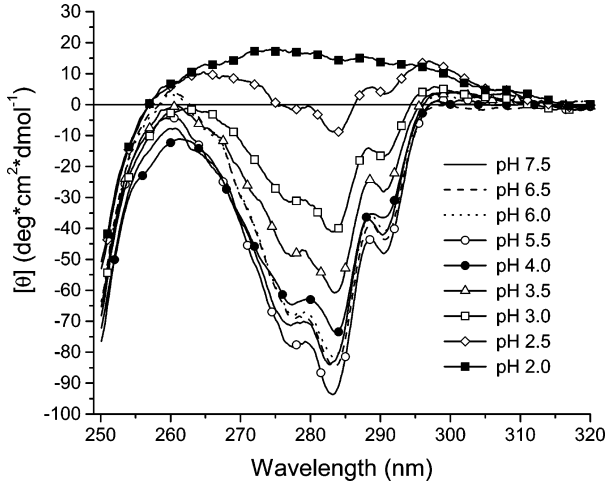

FIGURE 2: Near-UV CD spectra of apo-TL at various pH values.

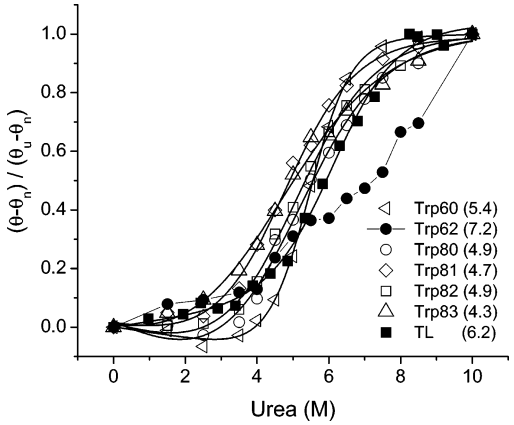

FIGURE 3: Denaturation of Trp mutants of TL in urea. TL is shown for comparison. The midpoints of transition for proteins are shown in parentheses.

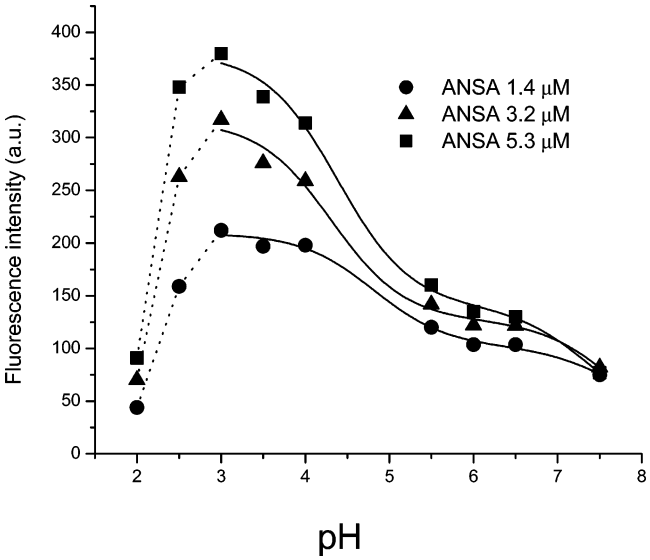

FIGURE 4: Fluorescence intensity of ANSA incubated with apo-TL (1.2 μM) at various pH values showing modes of binding.

retained. Acid-driven unfolding at pH 2.0 results in almost complete loss of aromatic side chain rigidity.

Here, we ascribe decreased near-UV CD intensity to decreased aromatic side chain rigidity, but one should keep in mind that loss of specific side chain interactions also influences the CD signal intensity. A variety of mechanisms may create an asymmetric environment for the chromophore and induce CD bands (*41*, *42*). The wavelength position and sharpness of aromatic CD bands in proteins are often strongly influenced by the environment of each side chain, e.g., hydrogen bonding, polar or charged groups, and polarizability.

Circular Dichroism of Loop Mutants. To obtain more precise information about the milieu surrounding specific loop positions, site-directed tryptophan mutagenesis of interstrand loops CD and EF was performed. Since W17Y was used as a template for all tryptophan mutants, it is important to note that the far-UV CD spectra of W17Y and its binding characteristics have been previously studied and are similar to those of TL (*35*). Further, far-UV CD measurements of all mutant proteins affirm that the mutations did not perturb the proteins' secondary structure (see the Supporting Information).

The influence of the interloop Trp mutations on the stability of the TL mutant proteins is evident from the fractional change of ellipticity with increasing urea concentration (Figure 3). The curves are quite similar in their shape for most of the mutants. However, Trp62 shows a marked shift in the midpoint of transition for protein unfolding to 7.2 M, reflecting increased stability in the presence of denaturing agent.

Circular Dichroism of Mutations Involving Both Loops CD and EF. The strategy to obtain measurements of interloop distances involved proteins with a mutation of tryptophan on one loop and a cysteine substitution for dansyl labeling on the other loop. As a reference point, proteins were engineered, each with one cysteine mutation of the EF loop and a Trp mutation at the midpoint of the D strand. The far-UV circular dichroism spectra of these proteins are almost superimposable and only slightly different from that of TL, indicating that these mutations did not perturb the overall structure of the protein (see the Supporting Information).

Influence of pH on ANSA Binding. The influence of pH on binding sites and the accompanying structural changes were studied with ANSA, a widely used fluorescent chemical for the detection of hydrophobic patches in proteins. The fluorescence intensity of ANSA incubated with apo-TL at varying pH is shown in Figure 4. Distinct modes of ANSA binding are suggested at different pH values because at least two sigmoidal curves with different parameters are needed for fitting the data points. Points below pH 3.0 were excluded from the fitting curve because apo-TL shows features of extensive denaturation (Figure 1) and the fluorescent intensity falls off dramatically (Figure 4). A significant increase in ANSA intensity occurs at low pH with a midpoint of transition at about 4.5. This value is close to the pK_a values for Asp and Glu, both charged residues at neutral pH. At pH 7.5 the fluorescent intensity of bound ANSA is low and reaches saturation at approximately equimolar concentrations of ANSA and TL. However, as the pH is reduced from 7.5 to 3.0, there is a 3−5-fold increase in fluorescence intensity of bound ANSA, and the increase of fluorescence intensity is enhanced with greater concentrations of ANSA (no saturation). The increased fluorescent intensity at low pH suggests that additional hydrophobic sites became available and/or the affinity for existing binding sites increased. These possibilities were investigated with ANSA titration at varying pH (see the Supporting Information).

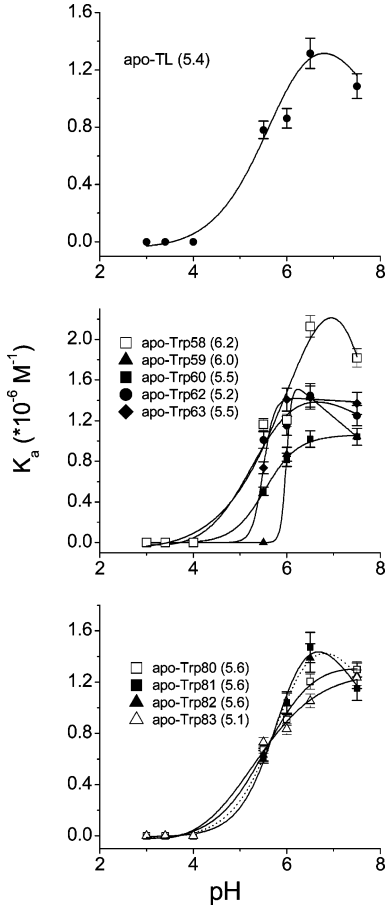

FIGURE 5: pH dependence of apparent binding constants for 16AP to apo-TL and apo-W mutants as shown. The midpoints of transitions for apoproteins are shown in parentheses.

Taken together, the results of the far- and near-UV CD and ANSA binding experiments show that apo-TL undergoes distinct conformational changes when the pH is decreased from 7.5 to 3.0 with the creation of additional binding sites for ANSA. At low pH, extracavitary binding of ANSA dominates while the secondary structure of the protein remains essentially intact. Denaturation of apo-TL occurs at pH below 3.0, which manifests as decreased fluorescence intensity of ANSA.

Influence of pH on the Binding Affinity of 16AP. 16AP is the fluorescent analogue of an endogenous ligand of TL, palmitic acid. Like palmitic acid, 16AP binds exclusively within the cavity (*35*). 16AP is suitable as a functional probe to study the relationship of conformational and structural changes of TL mutants to the fatty acid binding properties. 16AP-binding experiments were carried out at various pH values for each single tryptophan mutant to be sure pH-dependent ligand binding is maintained in the mutant proteins. The binding of 16AP with apo-TL and apo-W59 at varying pH is shown in the Supporting Information. The titration curves of 16AP with all other loop single Trp mutants are quite similar (data not shown).

The binding constants of 16AP for all single tryptophan mutants are plotted with respect to pH in Figure 5. There are properties that are common to all mutants and TL such as binding to 16AP in a broad region around neutral pH but not at pH $\leq$ 4.0. Also, from pH 4.0 to pH 6.5, all proteins show an increase in binding affinity with similar midpoints of transition to TL. But at pH 7.5 there is a slight but consistent decrease in binding affinity for most of the proteins tested. Of note W59 shows absence of binding at pH 5.5 and therefore has a steeper transition. The original residue in position 59 is Gly, which does not have a side chain, and Trp in that position is exposed to the solvent (*17*). Therefore, the loss of fatty acid binding at relatively greater pH values is not the result of a pK_a shift in neighboring titratable side chains but rather is probably due to the bulky side chain of Trp at position 59. This effect was not observed in the Trp substitutions for Gly in positions 81 and 82. Also, despite the fact that the loops CD and EF have the charged (at neutral pH) residues (Arg60, Glu63 and Asp80, Lys83, respectively), substitution with Trp at these sites did not shift the midpoint of transition significantly (Figure 5). The utilization of tryptophan substitutions as probes to study conformational changes with varying pH is justifiable for two reasons. First, over the specified pH range the far-UV CD structure is similar between mutants (Supporting Information). Second, the general features of pH-dependent binding of 16AP are not disrupted over the entire pH range. The differences in the binding curves are likely to reflect pH-dependent conformational changes resulting from environmental alterations induced by the mutations.

It is evident from Figure 5 that the pH dependencies of the binding affinity of 16AP to the apoproteins are not simple sigmoidal plots. Therefore, the loss of ligand binding to TL cannot be characterized as driven by a single titratable side chain. The data contrast that described for β-lactoglobulin where Glu89 acts as a protonation-induced trigger to close loop EF with concomitant loss of fatty acid binding (*21*). In TL, several titratable side chains are likely to be involved in direct gradual conformational and structural changes. These changes are reflected in the environment of individual residues.

Accessibility Studies of Interstrand Loop Residue Positions. Accessibility studies of single tryptophan mutants characterize the environmental differences for residues in the interstrand loops at pH 7.3 and 3.0. A typical Stern−Volmer plot that is representative of the quenching experiments with tryptophan mutants is shown in the Supporting Information. Typically, there is greater acrylamide quenching at pH 7.3 than at pH 3.0; exposure to solvent decreases at acidic pH. The fluorescence characteristics including acrylamide quenching data for all single Trp mutants are summarized in Figure 6 and Table 1. It is evident that accessibility is lower for all residues on the interstrand loops at pH 3.0 than at pH 7.3. The effect is much less for flanking residues of both loops. For every Trp mutant, except Trp80, the decrease in accessibilities correlates well with their blue shift in fluorescence λ_{max}. However, Trp80 shows a small increase in fluorescence λ_{max} compared to that of Trp81 despite the notable decrease in accessibility (pH 7.3). A charged residue near Trp80 may account for this discrepancy of λ_{max}. It is known that a positive charge near the benzene end or a negative charge near the pyrrole end of the Trp creates a red shift of fluorescence (*43*). Therefore, the large blue shift in fluorescence λ_{max} of Trp80 that is accompanied by a small decrease in accessibility is most likely due to the loss of a nearby charge that exists at pH 7.3 but not at pH 3.0. This may arise from either movement of a nearby charge group and/or protonation of titratable side chains (e.g., Glu or Asp).

Table 1: Fluorescence Parameters for Single Trp Mutants of TL

mutant	α_1	α_2	f_1	f_2	τ_1 (ns)	τ_2 (ns)	$\bar{\tau}$ (ns)	$\langle\tau\rangle$ (ns)	Q	$\kappa_r \times 10^{-6}$ (s^{-1})	f_{PR}	f_{DQ}	$\langle\tau\rangle_{pH3.0}/\langle\tau\rangle_{pH7.3}$	χ^2
Trp58, pH 7.3	0.59	0.41	0.37	0.63	2.26	5.55	4.33	3.61	0.13	36				2.4
Trp58, pH 3.0	0.61	0.39	0.29	0.71	0.96	3.70	2.91	2.03	0.07	34.5	0.98	0.57	0.56	1.6
Trp59, pH 7.3	0.60	0.40	0.36	0.64	1.39	3.72	2.88	2.32	0.07	30.2				2.7
Trp59, pH 3.0	0.75	0.25	0.39	0.61	0.72	3.36	2.33	1.38	0.03	21.7	0.85	0.70	0.59	1.7
Trp60, pH 7.3	0.55	0.45	0.26	0.74	1.01	3.49	2.85	2.13	0.09	42.3				1.3
Trp60, pH 3.0	0.76	0.24	0.43	0.57	0.84	3.51	2.36	1.48	0.05	33.8	0.76	0.92	0.69	1.5
Trp62, pH 7.3	0.62	0.38	0.36	0.64	1.31	3.74	2.87	2.23	0.10	44.8				2.3
Trp62, pH 3.0	0.64	0.36	0.34	0.66	0.92	3.17	2.41	1.73	0.07	40.5	0.98	0.79	0.78	1.0
Trp63, pH 7.3	0.55	0.45	0.28	0.72	1.49	4.74	3.83	2.95	0.11	37.3				1.7
Trp63, pH 3.0	0.68	0.32	0.38	0.62	1.15	3.94	2.88	2.04	0.07	34.3	0.86	0.81	0.69	1.7
Trp80, pH 7.3	0.32	0.68	0.11	0.89	1.85	7.14	6.56	5.45	0.23	42.2				0.9
Trp80, pH3.0	0.68	0.32	0.41	0.59	1.32	4.11	2.97	2.21	0.07	31.7	0.65	0.62	0.41	1.3
Trp81, pH 7.3	0.48	0.52	0.25	0.75	1.59	4.42	3.71	3.06	0.11	35.9				1.4
Trp81, pH 3.0	0.73	0.27	0.45	0.55	1.07	3.46	2.38	1.72	0.04	23.3	0.77	0.73	0.56	1.1
Trp82, pH 7.3	0.66	0.34	0.38	0.62	1.32	4.21	3.11	2.30	0.08	34.8				1.6
Trp82, pH 3.0	0.73	0.27	0.40	0.60	1.01	4.12	2.88	1.85	0.06	32.4	0.91	0.88	0.80	1.7
Trp83, pH 7.3	0.45	0.55	0.18	0.82	1.17	4.38	3.80	2.94	0.11	37.4				1.7
Trp83, pH 3.0	0.69	0.31	0.36	0.64	0.95	3.82	2.79	1.84	0.06	32.6	0.74	0.85	0.63	0.9

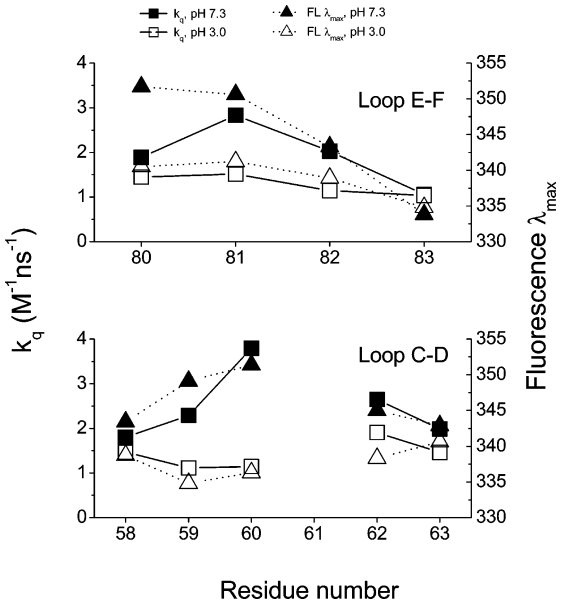

FIGURE 6: Maxima of the emission peaks (λ_{max}) of the corrected spectra and bimolecular collisional rate constants (k_q) of single Trp mutants of TL at pH values of 7.3 and 3.0.

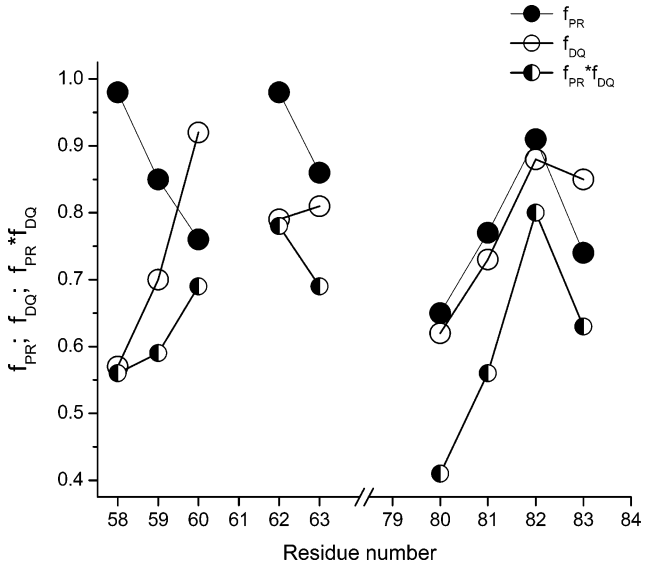

FIGURE 7: Fluorescence lifetime decrease ($\langle\tau\rangle/\langle\tau_0\rangle = f_{PR}f_{DQ}$), population reshuffling (f_{PR}), and pure dynamic quenching (f_{DQ}) parameters calculated for the single Trp mutants of TL in the transition from pH 7.3 to pH 3.0.

One possibility is that the protonated side chain is Glu69. In the TL model (*17*), Glu69 is in close proximity to Glu80 (distance between Cα atoms ~8.4 Å). In addition the lifetime of Trp80 decreases more than 2-fold in the transition from pH 7.3 to pH 3.0. Glu is known to be a weak quencher of tryptophan in the unprotonated form and becomes a strong quencher in the protonated (uncharged) state (*31*). At pH 3.0 Glu69 will be protonated. Further studies are needed to verify the importance of the possible specific interaction of Asp80 and Glu69 in pH-induced conformational changes.

The quantum yield and fluorescent lifetimes of tryptophans in different interstrand loop positions reveal differences about the protein environment at pH 7.3 versus pH 3.0. Both quantum yield and average fluorescent lifetime values decrease from pH 7.3 to pH 3.0, although to varying extents (Table 1). The radiative rate constants, k_r, for Trp residues in both loops at pH 3.0 and 7.0 are about the same order of magnitude and comparable to k_r values for 3-methylindole, tryptophan zwitterions, and *N*-acetyltryptophanamide ((40−60) × 10^6 s^{-1}) (*44*). The similarities in k_r values of Trp residues indicate that decreased quantum yields are due to dynamic quenching of Trp fluorescence by nearby groups. Two lifetime components characterized the fluorescence intensity decays, indicating two rotamer populations for Trp side chains. The range of fluorescent lifetimes for one rotamer is 0.72−2.26 ns, while the other is 3.17−7.14 ns.

The decreased average fluorescence lifetime of loop residues in the transition from pH 7.3 to pH 3.0 (Table 1) can be due to either a relative increase in the population with a shorter lifetime (population reshuffling) or shortening of individual lifetimes (pure dynamic quenching) (*45*). These parameters for the two loops show different characteristics (Table 1, Figure 7). The population reshuffling and pure dynamic quenching factors change in tandem for each individual residue along interstrand loop EF. Toward the flanking region, especially Trp80, one finds the greatest effect for both population reshuffling and pure dynamic quenching. At Trp82 both factors are closer to 1, i.e., very low population

Table 2: Fluorescence Resonance Energy Transfer Parameters

donor/acceptor	analysis[a]	α_1	α_2	τ_1 (ns)	τ_2 (ns)	$\langle\tau\rangle$ (ns)	χ^2	F	E	$J \times 10^{-13}$ ($M^{-1}\,cm^{-1}\,nm^4$)	R_0 (Å)	R (Å)
Trp62 (Cys81), pH 6.8	G	0.55	0.45	1.31	4.47	2.72						
Trp62/dansyl81, pH 6.8	G	0.55	0.45	1.06	4.52	2.6	1.3		0.043		18.8	~31.5
Trp62 (Cys81), pH 3.0	G	0.66	0.34	0.93	3.52	1.81						
Trp62/dansyl81, pH 3.0	G	0.66	0.34	0.61	3.07	1.45	1.4		0.20		18.6	23.4
Trp62 (Cys82), pH 6.8	G	0.64	0.36	1.49	4.77	2.68		0.074				
Trp62/dansyl82, pH 6.8	G	0.64	0.36	0.80	4.51	2.15	1.7		0.20	3.96	18.8	23.7
Trp62 (Cys82), pH 3.0	G	0.71	0.29	1.18	3.81	1.94		0.068				
Trp62/dansyl82, pH 3.0	G	0.71	0.29	0.61	3.20	1.36	1.6		0.30	3.98	18.6	21.4
Trp63 (Cys80), pH 6.8	NG	0.46	0.54	1.01	4.58	2.92	1.5	0.084				
Trp63/dansyl80, pH 6.8	NG	0.82	0.18	0.56	4.31	1.22	1.5		0.58	3.83	19.1	18.1
Trp63 (Cys80), pH 3.0	NG	0.62	0.38	1.03	3.85	2.10	1.5	0.063				
Trp63/dansyl80, pH 3.0	NG	0.74	0.26	0.60	3.5	1.44	1.8		0.31	3.94	18.3	20.9
Trp67 (Cys81), pH 6.8	NG	0.53	0.47	1.14	4.24	2.59	1.5	0.087				
Trp67/dansyl81, pH 6.8	NG	0.85	0.15	0.43	3.72	0.91	1.8		0.65	3.98	19.2	17.3
Trp67 (Cys81), pH 3.0	G	0.78	0.22	1.58	4.52	2.22		0.079				
Trp67/dansyl81, pH 3.0	G	0.78	0.22	0.63	3.27	1.20	1.6		0.46	3.82	19.1	19.6
Trp67 (Cys82), pH 6.8	G	0.82	0.18	2.56	6.60	3.28						
Trp67/dansyl82, pH 6.8	G	0.82	0.18	0.58	4.18	1.22	2.2		0.63		19.2	17.6
Trp67 (Cys82), pH 3.0	G	0.75	0.25	1.57	4.14	2.21						
Trp67/dansyl82, pH 3.0	G	0.75	0.25	0.60	3.13	1.24	1.2		0.44		19.1	19.8

[a] G = global analysis; NG = nonglobal analysis.

reshuffling and pure dynamic quenching. Therefore, the change in accessibility seen for Trp82 did not produce either a change in the rotamer population or apposition to a more efficient quenching group.

The characteristics of loops EF and CD differ. Overall, the CD loop shows less population reshuffling in the transition to acidic pH; four out of five residues have the f_{PR} value ≥ 0.85 (Table 1). In contrast three residues out of four of the loop EF have the f_{PR} value ≤ 0.77. One explanation is that the loop CD exhibits restricted backbone motion because the adjacent cysteine (Cys61) is joined in a disulfide bond. Reduced accessibility for the loop CD in the pH transition can be explained by movement of neighboring groups toward the loop CD.

Relative Distances between Interstrand Loop (CD and EF) Residues by RET. The accessibility and dynamic quenching data for residues along both interstrand loops suggest that the relative positions of the loops change in response to pH. The distance between residues on apposing strands was determined by resonance energy transfer using a Trp (donor) on one strand and a dansyl-labeled cysteine (acceptor) on the other.

Examples of frequency domain intensity decay curves for selected mutants at pH 6.8 and 3.0 are shown in Figures 8 and 9. The lifetime data and RET parameters are shown in Table 2. For some of the mutants the data could be fit by global analysis.

Inspection of the decay curves for W62C81 at pH 6.8 shows that the addition of the dansyl group has little effect on the lifetimes; there is no significant energy transfer (Figure 8A). The differences seen at pH 3.0 (Figure 8B) indicate that the donor and acceptor have moved closer, resulting in higher efficiency RET. The situation for W67C82 is quite different (Figure 9). At pH 6.8 there is a marked difference in the decay curves that reflects RET. The difference is mitigated at pH 3.0. The Trp and dansyl group have moved further apart. Trp67 is not part of the loop but rather is part of the strand D (*17*).

A diagramatic summary of the relative positions of the residues from the interstrand loops is depicted in Figure 10. The residues of the CD loop are illustrated as stationary because the adjacent disulfide bond at residue 61 should restrain its motion.

The dynamic changes in the environment of the loops and motion of the loops and the change in binding affinity are correlated with pH changes in Figure 11. The pH titration was performed by plotting λ_{max}, since this parameter is very sensitive to electrostatic interactions (Figure 11). The graphs for λ_{max} of loop CD positions fit the Hendersen−Hasselbalch equation for one titration group. The greatest changes occur between pH 4.0 and pH about 6.5. It is also evident that there is great variability among individual residues in the pH values associated with changes in λ_{max}. The computed apparent pK_a values reflect the marked differences of the environments at each point along both loops. For the CD loop mutants W60 and W62 the pK_a values, 4.3 and 4.5, respectively, are quite close to those of residues with carboxylic acid side chains, suggesting an adjacent Glu or Asp. However, the magnitude of $\Delta\lambda_{max}$ over the transition from pH 7.3 to pH 3.0 is about 3.6-fold greater for position 60 compared to position 62. It is possible that the positively charged Arg side chain at position 60 suppresses changes in λ_{max} of Trp62. This interaction implies that the positive charge of Arg and the negative charge of Glu or Asp are both positioned at the pyrrole end of tryptophan.

The pK_a values for tryptophan at positions 60 and 62 are different from that for tryptophan at position 59 in which the pK_a value is shifted (6.2), perhaps suggesting a nearby His or an anomalous Glu or Asp. The pK_a^1 values for W81 and W82 suggest a nearby carboxylic acid side chain. The pK_a^2 values may be explained by the adjacent His 84 (pK_a-(His) $\approx$ 6.0). Interestingly, position 59 is occupied by glycine in TL, and its pK_a value is similar to the λ_{max} pK_a^2 values observed for positions 81 and 82 of the EF loop, which also contain glycine. Because neither glycine nor tryptophan contains a charged side chain, the tryptophan mutation is unlikely to affect the ionization properties of the local environments at these positions. Therefore, the distinctive nature of each curve of λ_{max} reflects the variation in local responses at each residue of the loops.

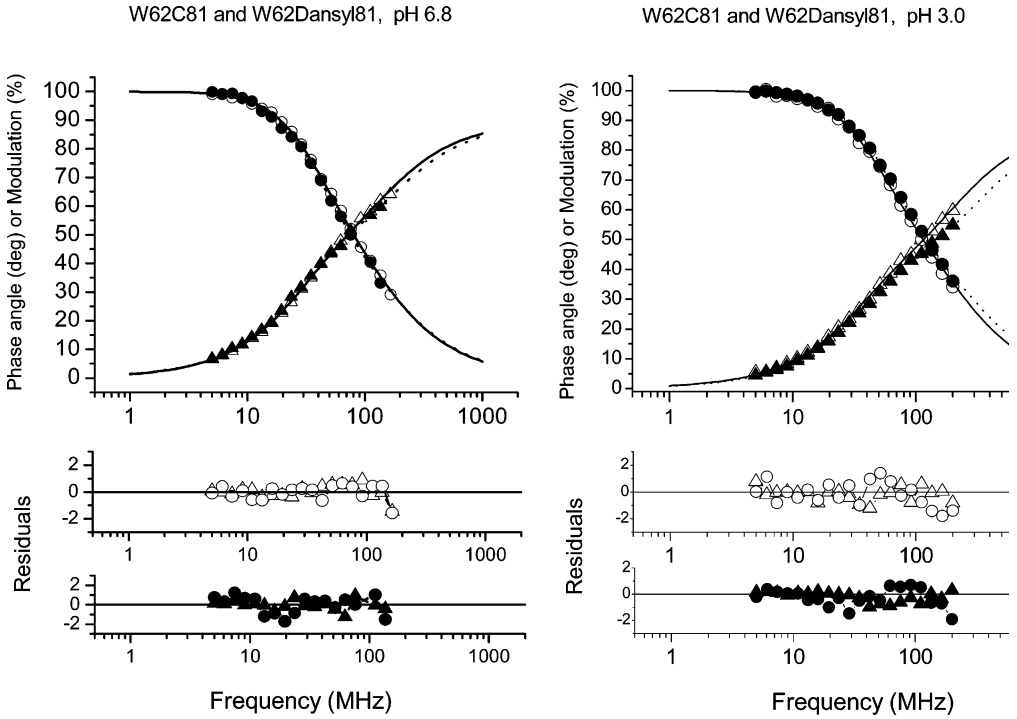

FIGURE 8: Phase angle (triangles) and modulation (circles) fluorescence lifetime data of TL mutant W62C81, dansyl-labeled Cys81 (solid symbols), and unlabeled Cys81 (open symbols) for detection of RET at pH 6.8 and 3.0. Lines represent the best biexponential fit for the parameters given in Table 2.

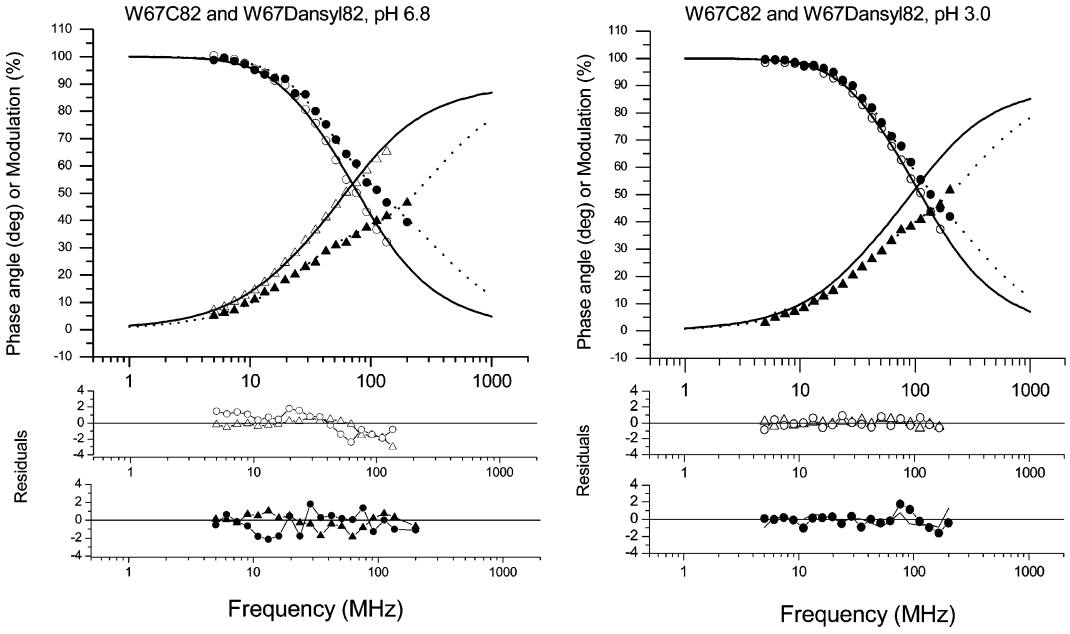

FIGURE 9: Phase angle (triangles) and modulation (circles) fluorescence lifetime data of TL mutant W67C82 with dansyl-labeled Cys82 (solid symbols) and unlabeled (open symbols) for detection of RET at pH 6.8 and 3.0. Lines represent the best biexponential fit for the parameters given in Table 2.

Several lines of evidence suggest that the mechanism of pH-dependent ligand binding is not attributable to a single titratable group acting as a trigger. First, the pK_a for λ_{max} varies at positions along the loop. Each tryptophan mutation senses a unique microenvironment with a different local response to pH. Second, the titration curves for λ_{max} vary in shape for each residue, and those of the EF loop cannot be characterized as simple sigmoidal plots that would be expected in the case of a single titratable group. Third, mutations at each position along the loop do not perturb the pH-dependent ligand binding as would be expected if a single titratable residue were critical to the process.

CONCLUSION

The application of site-directed tryptophan fluorescence distinguishes pH-induced local environmental changes along the loops EF and CD from that of overall structure and reveals important clues about the mechanism of pH-induced ligand release in TL.

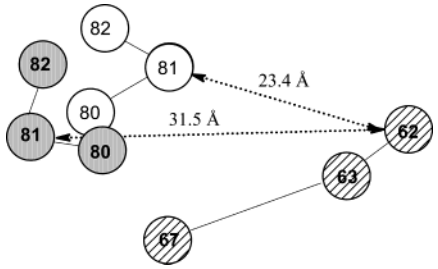

FIGURE 10: Diagram of the changes in the relative positions of the residues from the interstrand loops EF and CD in the transition from pH 7.3 (shaded circles) to pH 3.0 (open circles). Residues 62, 63, and 67 (striped circles) are shown in a stable reference position.

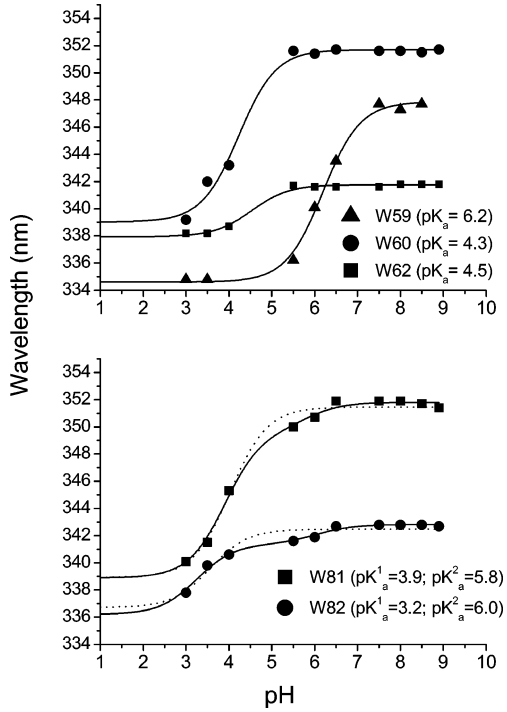

FIGURE 11: λ_{max} for single Trp mutants of TL at various pH values. The pK_a values are shown in parentheses. The dashed lines for W81 and W82 represent fitting curves for a single titratable group in the Hendersen−Hasselbalch equation.

From pH 7.5 to pH 6.5, ligand affinity is not reduced and there is no significant change in either secondary structure or the λ_{max} of tryptophans at four of the five loop positions.

From pH 6.5 to pH 5.5, ligand release is initiated as evident by decreased affinity for TL (midpoint of transition for K_a of ~5.9 for 16AP). The pK_a value for λ_{max} (5.7) of residue 59 closely corresponds to the midpoint of transition of ligand affinity. The essentially unaltered CD spectra imply that ligand release cannot be attributed to relaxation either in secondary structure or in the conformational state in the lipocalin core.

From pH 5.5 to pH 3.0, there is progressive loss of intracavitary ligand binding. There is an accompanying decrease in accessibility for residues on both loops. In addition, at pH 5.5−3.0 there is relaxation of secondary structure and decreased aromatic side chain rigidity (Figures 1 and 2) that can contribute to the complete loss of intracavitary binding.

Decreasing pH induces apposition of the EF and CD loops corresponding to a more buried position of the side chains of amino acids on both loops and steric restriction of ligand access. The mechanism of pH-induced ligand release for TL appears to differ from that of β-lactoglobulin. In β-lactoglobulin a single titratable group is considered the trigger for loop movement and fatty acid binding. The overall impression is that pH-induced ligand release in TL is a cascade of events starting with sequentially recruited side chains of varying pK_a. The pH-driven changes in ionization states promote apposition of loops CD and EF over the entrance to the calyx.

ACKNOWLEDGMENT

We thank Dr. Joseph Horwitz for access to the CD instrument.

SUPPORTING INFORMATION AVAILABLE

Detailed methods of the expression and purification of mutant proteins, calculation of the quantum yield, fluorescent lifetime measurements, distance measurements by RET, far-UV CD spectra of Trp and Trp/Cys mutants at pH 2.0−7.5, far-UV CD spectra of W17Y and TL at pH 7.5, ANSA binding to apo-TL at various pH values, competition of the ANSA-binding site of apo-TL by stearic acid at pH 7.3 and 3.0, 16AP binding to apo-TL and apo-W59, and acrylamide quenching of Trp fluorescence for mutant protein W81, pH 7.3 and 3.0. This material is available free of charge via the Internet at http://pubs.acs.org.

REFERENCES

1. Glasgow, B. J., Abduragimov, A. R., Farahbakhsh, Z. T., Faull, K. F., and Hubbell, W. L. (1995) Tear lipocalins bind a broad array of lipid ligands, *Curr. Eye Res. 14*, 363−372.
2. Glasgow, B. J., Marshall, G., Gasymov, O. K., Abduragimov, A. R., Yusifov, T. N., and Knobler, C. M. (1999) Tear lipocalins: potential lipid scavengers for the corneal surface, *Invest. Ophthalmol. Visual Sci. 40*, 3100−3107.
3. Selsted, M. E., and Martinez, R. J. (1982) Isolation and purification of bactericides from human tears, *Exp. Eye. Res. 34*, 305−318.
4. van't Hof, W., Blankenvoorde, M. F., Veerman, E. C., and Amerongen, A. V. (1997) The salivary lipocalin von Ebner's gland protein is a cysteine proteinase inhibitor, *J. Biol. Chem. 272*, 1837−1841.
5. Blaker, M., Kock, K., Ahlers, C., Buck, F., and Schmale, H. (1993) Molecular cloning of human von Ebner's gland protein, a member of the lipocalin superfamily highly expressed in lingual salivary glands, *Biochim. Biophys. Acta 1172*, 131−137.
6. Redl, B., Holzfeind, P., and Lottspeich, F. (1992) cDNA cloning and sequencing reveals human tear prealbumin to be a member of the lipophilic-ligand carrier protein superfamily, *J. Biol. Chem. 267*, 20282−20287.
7. Lechner, M., Wojnar, P., and Redl, B. (2001) Human tear lipocalin acts as an oxidative-stress-induced scavenger of potentially harmful lipid peroxidation products in a cell culture system, *Biochem. J. 356*, 129−135.
8. Glasgow, B. J., Abduragimov, A. R., Gassymov, O. K., Yusifov, T. N., Ruth, E. C., and Faull, K. F. (2002) Vitamin E associated with the lipocalin fraction of human tears, *Adv. Exp. Med. Biol. 506*, 567−572.
9. Yusifov, T. N., Abduragimov, A. R., Gasymov, O. K., and Glasgow, B. J. (2000) Endonuclease activity in lipocalins, *Biochem. J. 347 Pt 3*, 815−819.
10. Flower, D. R. (1996) The lipocalin protein family: structure and function, *Biochem. J. 318* (Part 1), 1−14.
11. Gasymov, O. K., Abduragimov, A. R., Yusifov, T. N., and Glasgow, B. J. (2000) Resolution of ligand positions by site-directed tryptophan fluorescence in tear lipocalin, *Protein Sci. 9*, 325−331.
12. Glasgow, B. J., Abduragimov, A. R., Yusifov, T. N., Gasymov, O. K., Horwitz, J., Hubbell, W. L., and Faull, K. F. (1998) A conserved disulfide motif in human tear lipocalins influences ligand binding, *Biochemistry 37*, 2215−2225.

13. Gasymov, O. K., Abduragimov, A. R., Yusifov, T. N., and Glasgow, B. J. (2002) RET and anisotropy measurements establish the proximity of the conserved Trp17 to Ile98 and Phe99 of tear lipocalin, *Biochemistry 41*, 8837−8848.
14. Kennedy, M. W., Brass, A., McCruden, A. B., Price, N. C., Kelly, S. M., and Cooper, A. (1995) The ABA-1 allergen of the parasitic nematode Ascaris suum: fatty acid and retinoid binding function and structural characterization, *Biochemistry 34*, 6700−6710.
15. Narayan, M., and Berliner, L. J. (1997) Fatty acids and retinoids bind independently and simultaneously to beta-lactoglobulin, *Biochemistry 36*, 1906−1911.
16. Abduragimov, A. R., Gasymov, O. K., Yusifov, T. N., and Glasgow, B. J. (2000) Functional cavity dimensions of tear lipocalin, *Curr. Eye Res. 21*, 824−832.
17. Gasymov, O. K., Abduragimov, A. R., Yusifov, T. N., and Glasgow, B. J. (2001) Site-directed tryptophan fluorescence reveals the solution structure of tear lipocalin: evidence for features that confer promiscuity in ligand binding, *Biochemistry 40*, 14754−14762.
18. Gasymov, O. K., Abduragimov, A. R., Gasimov, E. O., Yusifov, T. N., Dooley, A. N., and Glasgow, B. J. (2004) Tear lipocalin: potential for selective delivery of rifampin, *Biochim. Biophys. Acta 1688*, 102−111.
19. Gasymov, O. K., Abduragimov, A. R., Yusifov, T. N., and Glasgow, B. J. (1998) Structural changes in human tear lipocalins associated with lipid binding, *Biochim. Biophys. Acta 1386*, 145−156.
20. Prats, M., Teissie, J., Tocanne J. F. (1986) Lateral proton conduction at lipid-water interfaces and its implications for the chemiosmotic-coupling hypothesis, *Nature 322*, 756−758.
21. Ragona, L., Fogolari, F., Catalano, M., Ugolini, R., Zetta, L., and Molinari, H. (2003) EF loop conformational change triggers ligand binding in beta-lactoglobulins, *J. Biol. Chem. 278*, 38840−38846.
22. Tanford, C. (1959) The reversible transformation of B-lactoglobulin at pH 7.5, *J. Am. Chem. Soc. 81*, 4032−4036.
23. Eberini, I., Baptista, A. M., Gianazza, E., Fraternali, F., and Beringhelli, T. (2004) Reorganization in apo- and holo-beta-lactoglobulin upon protonation of Glu89: molecular dynamics and pKa calculations, *Proteins 54*, 744−758.
24. Collini, M., D′Alfonso, L., Molinari, H., Ragona, L., Catalano, M., and Baldini, G. (2003) Competitive binding of fatty acids and the fluorescent probe 1-8-anilinonaphthalene sulfonate to bovine beta-lactoglobulin, *Protein Sci. 12*, 1596−1603.
25. Calderone, V., Berni, R., and Zanotti, G. (2003) High-resolution structures of retinol-binding protein in complex with retinol: pH-induced protein structural changes in the crystal state, *J. Mol. Biol. 329*, 841−850.
26. Clore, G. M., and Gronenborn, A. M. (1997) NMR structures of proteins and protein complexes beyond 20,000 M(r), *Nat. Struct. Biol. 4* (Suppl.), 849−853.
27. Glasgow, B. J., Gasymov, O. K., Abduragimov, A. R., Yusifov, T. N., Altenbach, C., and Hubbell, W. L. (1999) Side chain mobility and ligand interactions of the G strand of tear lipocalins by site-directed spin labeling, *Biochemistry 38*, 13707−13716.
28. Bychkova, V. E., Berni, R., Rossi, G. L., Kutyshenko, V. P., and Ptitsyn, O. B. (1992) Retinol-binding protein is in the molten globule state at low pH, *Biochemistry 31*, 7566−7571.
29. Gasymov, O. K., Abduragimov, A. R., Yusifov, T. N., and Glasgow, B. J. (1997) Solution structure by site directed tryptophan fluorescence in tear lipocalin, *Biochem. Biophys. Res. Commun. 239*, 191−196.
30. Adams, P. D., Chen, Y., Ma, K., Zagorski, M. G., Sonnichsen, F. D., McLaughlin, M. L., and Barkley, M. D. (2002) Intramolecular quenching of tryptophan fluorescence by the peptide bond in cyclic hexapeptides, *J. Am. Chem. Soc. 124*, 9278−9286.
31. Chen, Y., and Barkley, M. D. (1998) Toward understanding tryptophan fluorescence in proteins, *Biochemistry 37*, 9976−9982.
32. Glasgow, B. J., Heinzmann, C., Kojis, T., Sparkes, R. S., Mohandas, T., and Bateman, J. B. (1993) Assignment of tear lipocalin gene to human chromosome 9q34-9qter, *Curr. Eye Res. 12*, 1019−1023.
33. Glasgow, B. J. (1995) Tissue expression of lipocalins in human lacrimal and von Ebner's glands: colocalization with lysozyme, *Graefe's Arch. Clin. Exp. Ophthalmol. 233*, 513−522.
34. Cormack, B. (1987) *Current Protocol in Molecular Biology*, Vol. Suppl. 15, Greene Publishing Associates and Wiley- Interscience, New York.
35. Gasymov, O. K., Abduragimov, A. R., Yusifov, T. N., and Glasgow, B. J. (1999) Binding studies of tear lipocalin: the role of the conserved tryptophan in maintaining structure, stability and ligand affinity, *Biochim. Biophys. Acta 1433*, 307−320.
36. Marston, F. A. O. (1987) *A Practical Approach. In DNA Cloning*, Vol. III, IRL Press, Oxford, England.
37. Bozimowski, D., Artiss, J. D., and Zak, B. (1985) The variable reagent blank: protein determination as a model, *J. Clin. Chem. Clin. Biochem. 23*, 683−689.
38. Cogan, U., Kopelman, M., Mokady, S., and Shinitzky, M. (1976) Binding affinities of retinol and related compounds to retinol binding proteins, *Eur. J. Biochem. 65*, 71−78.
39. Eftink, M. R., and Ghiron, C. A. (1976) Exposure of tryptophanyl residues in proteins. Quantitative determination by fluorescence quenching studies, *Biochemistry 15*, 672−680.
40. Kuppens, S., Hellings, M., Jordens, J., Verheyden, S., and Engelborghs, Y. (2003) Conformational states of the switch I region of Ha-ras-p21 in hinge residue mutants studied by fluorescence lifetime and fluorescence anisotropy measurements, *Protein Sci. 12*, 930−938.
41. Gasymov, O. K., Abduragimov, A. R., Yusifov, T. N., and Glasgow, B. J. (2003) Resolving near-ultraviolet circular dichroism spectra of single trp mutants in tear lipocalin, *Anal. Biochem. 318*, 300−308.
42. Strickland, E. H. (1974) Aromatic contributions to circular dichroism spectra of proteins, *CRC Crit. Rev. Biochem. 2*, 113−175.
43. Vivian, J. T., and Callis, P. R. (2001) Mechanisms of tryptophan fluorescence shifts in proteins, *Biophys. J. 80*, 2093-2109.
44. Chen, Y. L. B., Yu, H. T., Barkley, M. D. (1996) *J. Am. Chem. Soc. 118*, 9271−9278.
45. Kuppens, S., Diaz, J. F., and Engelborghs, Y. (1999) Characterization of the hinges of the effector loop in the reaction pathway of the activation of ras-proteins. Kinetics of binding of beryllium trifluoride to V29G and I36G mutants of Ha-ras-p21, *Protein Sci. 8*, 1860−1866.

BI049076O